

Water Resources Research®



RESEARCH ARTICLE

10.1029/2021WR030052

Physics of Viscous Bridges in Soil Biological Hotspots

P. Benard¹ , J. R. Schepers² , M. Crosta^{3,4}, M. Zarebanadkouki⁵ , and A. Carminati¹ 

Key Point:

- Physical alterations of soil water by the release of highly polymeric substances promotes liquid connectivity in soil biological hotspots

¹Department of Environmental Systems Science, Physics of Soils and Terrestrial Ecosystems, ETH Zürich, Zürich, Switzerland, ²Department of Environmental Sciences, Plant Ecology and Evolution, University of Basel, Basel, Switzerland, ³Research Centre for Animal Production and Aquaculture, Council for Agricultural Research and Analysis of Agricultural Economics (CREA), Lodi, Italy, ⁴Università Cattolica, Piacenza, Italy, ⁵Chair of Soil Physics, University of Bayreuth, Bayreuth, Germany

Supporting Information:

Supporting Information may be found in the online version of this article.

Correspondence to:

P. Benard,
pascal.benard@usys.ethz.ch

Citation:

Benard, P., Schepers, J. R., Crosta, M., Zarebanadkouki, M., & Carminati, A. (2021). Physics of viscous bridges in soil biological hotspots. *Water Resources Research*, 57, e2021WR030052. <https://doi.org/10.1029/2021WR030052>

Received 24 MAR 2021

Accepted 24 OCT 2021

Abstract Plant roots and bacteria alter the soil physical properties by releasing polymeric blends into the soil pore space (e.g., extracellular polymeric substances and mucilage). The physical mechanisms by which these substances interact with the soil matrix and alter the spatial configuration of the liquid phase and the related hydraulic properties remain unclear. Here, we propose a theory to explain how polymer solutions form one-dimensional filaments and two-dimensional interconnected structures spanning across multiple pores. Unlike water, primarily shaped by surface tension, these polymeric structures remain connected during drying due to their high viscosity. The integrity of one-dimensional structures is explained by the interplay of viscosity and surface tension forces (elegantly characterized by the *Ohnesorge* number), while the formation of two-dimensional structures requires consideration of the interaction of the polymer solution with the solid surfaces and external drivers (e.g., drying rate). During drying, the viscosity of the liquid phase increases and at a critical point, when the friction between polymers and solid surfaces overcomes the water absorption of the polymers, the concentration of the polymer solution at the gas-liquid interface increases asymptotically. At this critical point, polymers are deposited as two-dimensional surfaces, such as hollow cylinders or interconnected surfaces. A model is introduced to predict the formation of such structures. Viscosity of the soil solution, specific soil surface, and drying rate are the key parameters determining the transition from one- to two-dimensional structures. Model results are in good agreement with observed structures formed in porous media during drying.

1. Introduction

Temporally and spatially confined, the rhizosphere is crossed by immense volumes of water (Bengough, 2012) while plant roots and microorganisms enhance biogeochemical fluxes, which turn this thin layer of soil around the roots into a distinct example of a hotspot in soil (Kuzaykov & Blagodatskaya, 2015). By the release of a multitude of compounds (Walker et al., 2003), soil organisms engineer the physical properties of their soil surroundings (Benard et al., 2019; Flemming et al., 2016; Naveed et al., 2019). Prominent among these substances are highly polymeric substances, such as EPS (extracellular polymeric substances) and mucilage, which alter the physical properties of the soil solution (Naveed et al., 2019; Read & Gregory, 1997; Read et al., 1999; Stoodley et al., 2002). They increase liquid connectivity, water retention, hydraulic conductivity, and solute diffusion coefficient (Benard et al., 2019; Carminati et al., 2017; Zarebanadkouki et al., 2019). Although liquid connectivity in the soil is of vital importance for the transport and availability of elements (McClain et al., 2003), description of the mechanism by which EPS and mucilage impact the connectivity of soil water remains incomplete.

The polymeric blends released from the plant and bacterial species are highly diverse (Flemming & Wingender, 2001; Naveed et al., 2017), yet, they appear to share key physical traits which alter the forces holding water in soils. Their high polymer content increases the viscosity of the liquid phase (Flemming & Wingender, 2001, 2010; Naveed et al., 2017; Stoodley et al., 2002), polymers can form a network (Flemming & Wingender, 2010; McCully & Boyer, 1997; Roberson et al., 1993) capable of absorbing and holding water (Flemming & Wingender, 2001; McCully & Boyer, 1997; Read et al., 1999; Roberson & Firestone, 1992; Segura-Campos et al., 2014), and surfactants among exuded polymers decrease the surface tension at the gas-liquid interface (Raaijmakers et al., 2010; Read et al., 2003). These three physical properties improve the connectivity of the liquid phase by avoiding the breakup of liquid connections in drying soils, finally resulting in the formation of long persistent strands between distant particles and wider hollow cylinders

© 2021. The Authors.

This is an open access article under the terms of the [Creative Commons Attribution License](https://creativecommons.org/licenses/by/4.0/), which permits use, distribution and reproduction in any medium, provided the original work is properly cited.

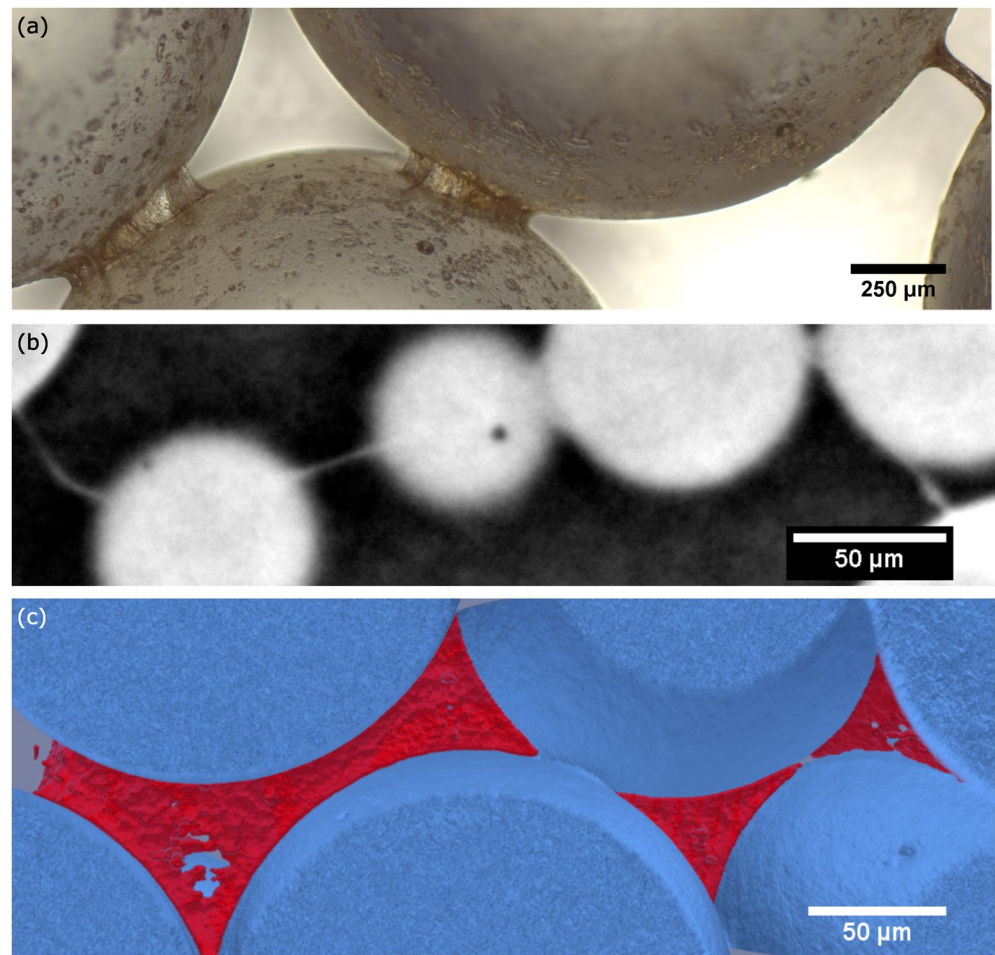


Figure 1. Dry maize (*Zea mays* L.) mucilage structures in glass beads. (a) Seedling maize mucilage with an initial concentration of 10 mg g^{-1} dried in glass beads of 1.7–2 mm in diameter. (b) Cross-section through a synchrotron-based X-ray tomographic microscopy volume of glass beads (0.1–0.2 mm in diameter) and dry crown root maize (*Zea mays* L.) mucilage structures (initial concentration 30 mg g^{-1}). (c) 3D segmentation of (b) with mucilage and glass beads shown in red and blue, respectively. At high mucilage content, the radius of mucilage structures approaches the glass bead radius and structures like the ones shown in (a) merge into 2D interconnected surfaces. Images (b and c) were adapted from Benard et al. (2019).

between nearby particles (e.g., Figure 1a). At high polymer concentration or high viscosity of the polymer solution, the hollow cylinders are larger than particles and merge into interconnected 2D surfaces (Figures 1b and 1c, Benard et al., 2019), with a transition of the deposited structures from the pendular to the funicular regime. The classical assumption of soil water being shaped by capillary and adsorptive forces (Tuller et al., 1999) cannot explain observed filaments and thin surfaces. The formation of filaments was explained by the interplay of viscosity, inertia, and surface tension (Carminati et al., 2017), yet, the forces involved in the creation of more extensive structures remain unclear.

Albalasmeh and Ghezzehei (2014) have discussed the role of hollow cylinders for the mechanical stability of particle pairs. They assumed that there is a critical concentration at which polymers are deposited and form a pendular ring. Here, we propose a conceptual model to predict this critical concentration.

We first review the existing literature on filaments (which have been extensively studied) and then focus on explaining the formation of 2D surfaces, such as hollow cylinders, using a conceptual model, tailored experiments and numerical simulations, followed by a brief discussion on their implications.

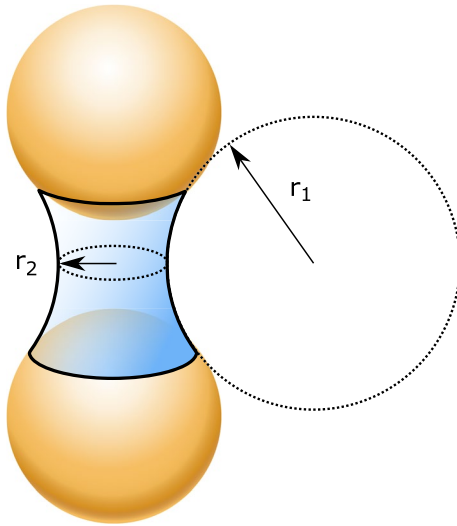


Figure 2. Principal radii of curvature r_1 and r_2 of a pendular liquid bridge.

2. Conceptual Model

The pendular bridge of water between two soil particles is shaped by surface tension which determines the work needed to stretch the gas-liquid interface. The curvature of such bridge relates to surface tension according to the Young-Laplace equation:

$$h_{\text{cap}} = \sigma \left(\frac{1}{r_1} + \frac{1}{r_2} \right) \quad (1)$$

where $h_{\text{cap}} = P_w - P_a$ [Pa] is the pressure difference between the liquid (P_w) and the gas phase (P_a), σ is the surface tension of the gas-liquid interface [mN m^{-1}], and r_1 and r_2 [m] being the principal radii of curvature, with r_1 being negative and r_2 being positive (Figure 2). During drying, the liquid bridge thins, r_2 becomes smaller and h_{cap} increases until it becomes positive. This leads to the Rayleigh-Plateau instability and the breakup of the bridge. The characteristic time of the breakup is milliseconds. The addition of polymeric substances, like mucilage, lowers the water potential of the liquid phase due to the absorptive potential provided by the polymer network, h_{ab} . The absorptive potential and surface tension are a function of polymer concentration in the liquid, c . Including the contribution of h_{ab} to the total water potential of the liquid bridge, h_{total} Equation 1 becomes:

$$h_{\text{total}} = \sigma(c) \left(\frac{1}{r_1} + \frac{1}{r_2} \right) + h_{\text{ab}}(c) \quad (2)$$

The water potential of a liquid bridge of varying volume is illustrated in Figure 3. The calculations are made for surface tension and absorptive forces reported for maize mucilage (Carminati et al., 2017) using Equation 2 to calculate the water potential based on an imposed capillary bridge. The change in water potential is plotted for three initial mucilage concentrations (mg dry mucilage per g of liquid). For water, at zero mucilage concentration surface tension causes rapid drainage followed by breakup of the liquid bridge at a water potential of about -10 hPa (0 mg g^{-1} , green line). A mucilage concentration of 1.6 mg g^{-1} results in a lower water content of the liquid bridge when compared to water due to the reduced surface tension (blue line). At the initial concentration of 16 mg g^{-1} , the absorptive potential (h_{ab}) dominates over surface tension, resulting in an increased water content at any water potential and a stable liquid bridge (purple line). At the initial concentration of 1.6 mg g^{-1} , the water potential has a maximum (a minimum in the figure as we have plotted minus the water potential) at a water content of ca. 0.015. As drying proceeds, the water potential decreases again due to an increase in polymer concentration hence decrease in absorptive potential. The part of the trajectory below the red dotted line is not in equilibrium (with an imaginary volume of bulk water connected to the bridge). In this region, the capillary pressure tends to become positive which, for water and inviscid liquids, would lead to the breakup of the bridge. The dynamics of thinning depend on the interplay of viscosity, inertia and surface tension (Eggers & Villermaux, 2008). The Ohnesorge number expresses the relative importance of surface tension vs. viscous forces and inertia in shaping such a liquid thread (Ohnesorge, 1936):

$$\text{Oh} = \frac{\eta}{\sqrt{\sigma \rho d}} \quad (3)$$

with viscosity η [Pa s], surface tension σ [N m^{-1}], liquid density ρ [kg m^{-3}], and filament diameter d [m]. The physics of filaments of polymer solutions is discussed in Carminati et al. (2017) and Ohnesorge (1936). For high Ohnesorge numbers, $\text{Oh} \gg 1$ viscosity dominates over surface tension and inertial forces and the thinning of the filament of a Newtonian viscous fluid is given by (McKinley & Tripathi, 2000; Sattler et al., 2012):

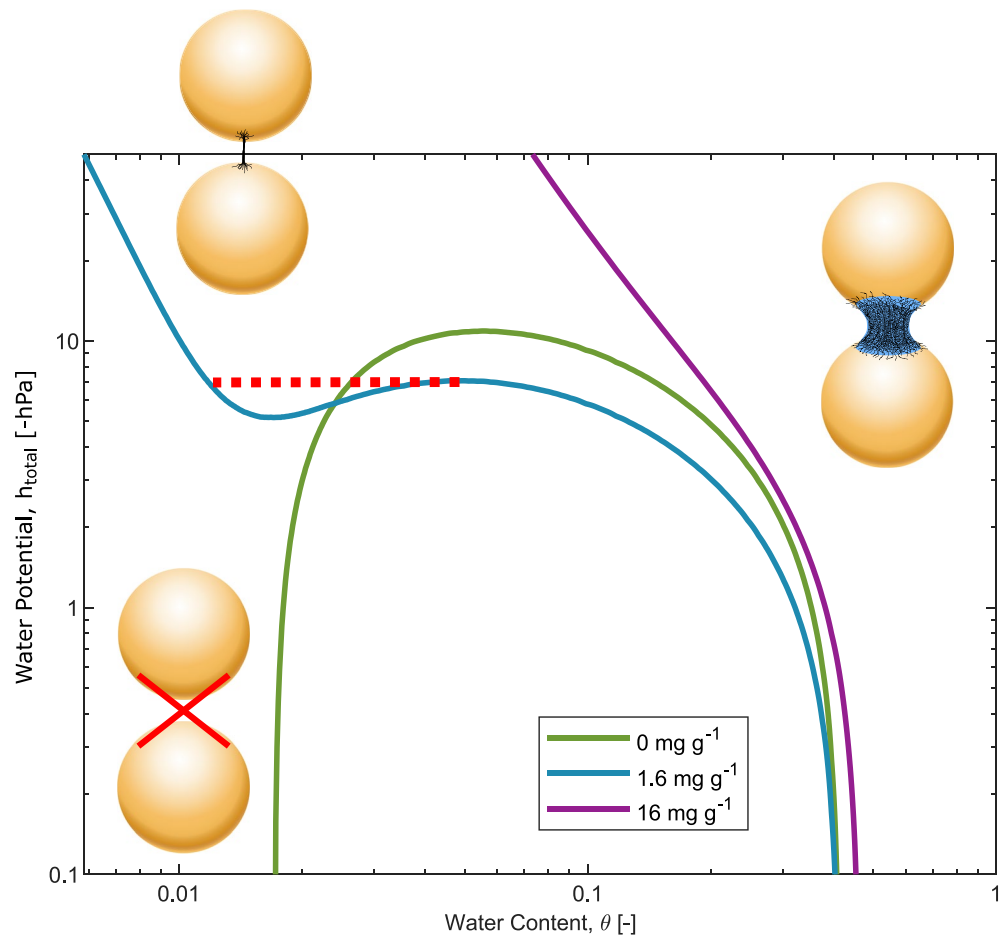


Figure 3. Water content of a pendular bridge between a pair of spheres as a function of water potential h_{total} with the absorptive part, h_{ab} [Pa] as a function of mucilage concentration C [mg g^{-1}] ($h_{\text{ab}} = -0.005725 (C)^{2.514}$; from Carminati et al., 2017). At 0 mg g^{-1} mucilage concentration (water), the liquid bridge is drained and breaks below a water content of about 0.05 (green curve). At 1.6 mg g^{-1} (blue line), the liquid bridge is drained but remains intact due to the decrease in water potential when mucilage is concentrated in the liquid during rapid drainage indicated by the dashed red line. At a comparably high initial mucilage concentration of 16 mg g^{-1} (purple line), large volumes of water are absorbed by mucilage preventing rapid drainage and resulting in an increased water content within the range of presented water potential.

$$\frac{dR}{dt} = 0.0709 \frac{\sigma}{\eta} \quad (4)$$

with filament radius R [m] and time t [s]. For polymer solutions, the thinning is accompanied by an increase in viscosity, eventually preventing the breakup of the liquid phase when $Oh \gg 1$ (Sattler et al., 2012). For polymer solutions in porous media, this leads to the formation of persistent thin thread-shaped structures upon drying (Carminati et al., 2017).

The concept above explains the impact of viscosity, surface tension and water absorption on the formation of persistent liquid filaments. However, a new conceptual model is needed to explain the formation of two-dimensional surfaces.

Consider a pair of two horizontal planes separated by a gap of length $2L$ and connected by a pendular bridge of liquid (Figure 4). We study the forces governing the concentration gradients of polymers in the solution. The idea is that two-dimensional surfaces are deposited where and when the concentration of polymers at the gas-liquid interface increases asymptotically. At this critical point, the polymers can no longer move and are deposited. Compared to Equations 1 and 2, which are applied to the bulk liquid (polymer solution

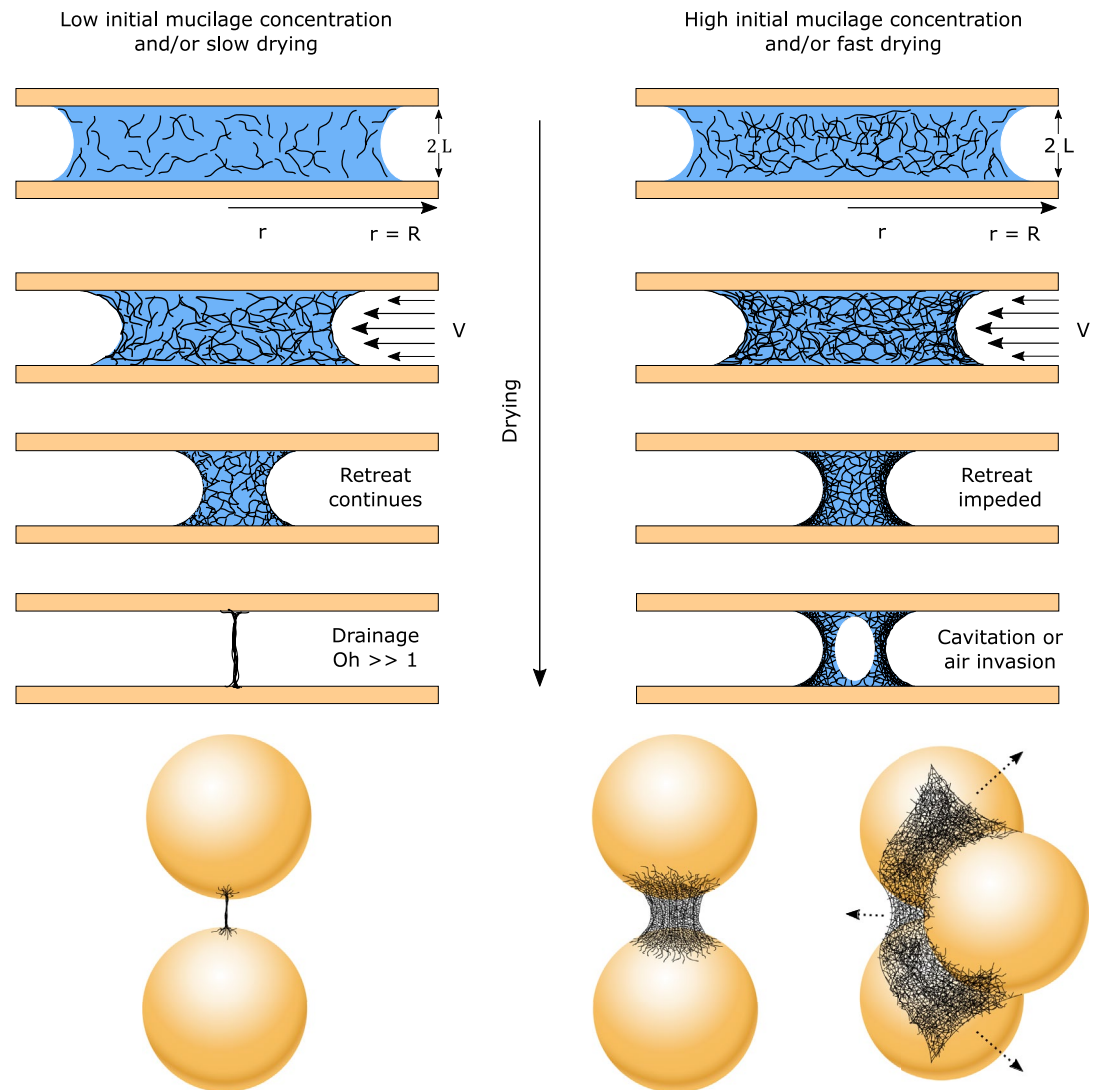


Figure 4. Concept of liquid retreat between particle pairs with surfaces represented by horizontal planes with distance $2L$, and impact of initial mucilage concentration and drying rate on their final diameter, R . At low initial mucilage concentration or at low drying rate, mucilage retreats until high viscosity ($Oh \gg 1$) results in the formation of thin filaments between particles (left side of the illustration). At high initial mucilage concentration and/or at high drying rate, mucilage retreat is eventually impeded by friction resulting in the formation of two-dimensional structures between particles (right side of the illustration).

with uniform concentration), here we explicitly consider the relative movement between water and the polymer network. We describe the forces acting on the polymer network. Upon drying, the gas-liquid interface recedes toward the center of the liquid bridge at $r = 0$, with r being the radial distance between the center of the circular bridge and the gas-liquid interface (at position $r = R$). As the interface recedes, the polymer network is stretched and its movement is governed by two key forces: one force is the resistance of the polymer network to flow, here considered as the friction between the polymers and the solid surfaces. The resistance to flow is calculated assuming a laminar flow parallel to the horizontal planes, null velocity at the liquid-solid contact (no-slip condition) and velocity v [m s^{-1}] at half distance between the plates. The friction F_f over the area $2\pi r \cdot dr$ is calculated as:

$$F_f = 4\pi r \cdot dr \cdot \eta \cdot \frac{v(r)}{L} \quad (5)$$

Note that this force is calculated for the friction against two surfaces (two planes), that η depends on the friction between polymers, that v is the velocity of the polymer network relative to the solid surface at mid distance between the two planes and that it is function of r , with v linearly decreasing in absolute values from its maximum at the gas-liquid interface at $r = R$, where it is equal to dR/dt , to zero at $r = 0$. Furthermore, v is negative for polymers moving toward $r = 0$. Equation 5 is defined for $0 \leq r \leq R$. In this equation, we implicitly assume that viscosity is primarily controlled by the properties of the polymer network (rather than those of the solvent—i.e., water) and that the network is viscous (rather than elastic). A more rigorous treatment would require the definition of specific properties of the network and the simulation of water and polymer network displacements, but this goes beyond the scope of this study.

Friction is opposed by a second force which drives the retreat of the polymer network from high concentrations at the gas-liquid interface ($r = R$) to low concentrations at the center of the bridge ($r = 0$). This gradient in concentration results in a gradient in absorptive water potential between the center (less negative water potential) and the gas-liquid interface (more negative water potential), which drives the motion of water relative to the polymer network toward the gas-liquid interface. At the same time, this force drives the polymers toward the center of the liquid bridge (where their concentration is the lowest). Note that this is a relative movement between water and polymer. The force of water absorption, F_a pulling water toward the gas-liquid interface is equal and opposite to the force pulling the polymers toward the center and it is equal to:

$$F_a = 2\pi r \cdot 2L \cdot dh_{ab} \quad (6)$$

where r [m] is the radial coordinate, $2L$ [m] is the distance between the horizontal planes and dh_{ab} is the difference in absorptive potential over the distance increment dr .

We calculate the critical point when friction impedes the receding of the polymer network by equating the two forces (Equations 5 and 6) in the region $0 \leq r \leq R$. Doing so, we obtain the equation:

$$\frac{\partial dh_{ab}}{\partial r} = \eta \cdot \frac{v(r)}{L^2} \quad (7)$$

As h_{ab} and η are functions of the concentration of the polymer network, C [g m^{-3}], Equation 7 becomes:

$$\frac{\partial dh_{ab}}{\partial C} \frac{\partial C}{\partial r} = \eta(C) \cdot \frac{v(r)}{L^2} \quad (8)$$

Equation 8 is solvable for constant L once the relations $h_{ab}(C)$ and $\eta(C)$ are given. Additionally, we have applied Equation 8 to approximately simulate the case of a pendular bridge between two spherical particles.

3. Numerical Implementation

The concept illustrated in Figure 4 is solved numerically by combining a pore morphological model (Hilpert & Miller, 2001) to determine the 3D liquid configuration between two spherical particles for decreasing soil water potential based on Equation 2 and the criterium for mucilage deposition obtained solving analytically Equation 8. Pore morphology models have been used to determine the capillary pressure-water saturation curve (Arand & Hesser, 2017; Chan & Govindaraju, 2011; Hilpert & Miller, 2001; Vogel et al., 2005). The idea is to represent porous media by a digital structure consisting of pores and solid particles. By successive morphological opening operations with spherical structural elements to water-filled pores the configuration of the liquid phase at a capillary pressure corresponding to the one calculated based on Equation 1 is derived.

In this model, the porous medium consists of two spheres with a radius of 75 μm , representing two soil particles with distance $2L$. We used this model to study the effect of varying initial mucilage concentration and particle distance $2L$ on the spatial configuration of the liquid phase during soil drying. The numerical procedure is implemented in Python (Version 3.9.6; Van Rossum & Drake, 2009) in the following way:

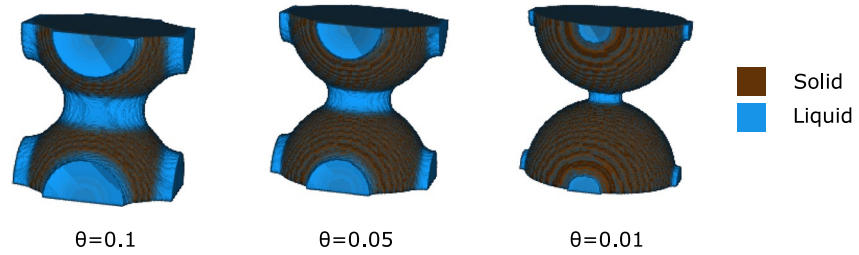


Figure 5. Representative illustration of liquid configuration at decreasing water content θ during pore drainage by use of a spherical structuring element for morphological opening.

1. The porous medium is discretized into equally sized voxels of $1 \mu\text{m}$ length.
2. The porous medium is initially saturated with the water potential of the liquid phase calculated based on Equation 2, assuming the first term (capillary pressure) being zero.
3. Morphological opening with a spherical structuring element of diameter D is performed on the water-filled space.
4. The two principal radii of curvature r_1 and r_2 are calculated based on the updated configuration of the liquid phase. To do so, r_1 is assumed to be equal to the diameter of the spherical structuring element used for morphological opening. The principal curvature of r_2 is calculated as the shortest distance from the central axis of the liquid bridge to the gas-liquid interface.
5. To derive the physical properties needed to determine whether friction impedes the retreat of the gas-liquid interface (Equation 8), the average concentration of mucilage, C in the liquid phase is determined based on its initial concentration in the previous step ($i-1$) and the ratio of change in the volume V of liquid (V_{i-1} / V_i) as follows:

$$C(i) = C(i-1) \frac{V_{i-1}}{V_i} \quad (9)$$

6. Distance $2L$ is updated after each iteration with regard to the current position of the gas-liquid interface along the spherical surfaces; this is considered as the point where friction is highest, due to the high velocity of the polymer network. Surface tension, viscosity, absorptive potential, and Ohnesorge number are updated after each iteration based on measured surface tension, viscosity and absorptive water potential curves parameterized using the following power laws

$$h_{ab}(i) = -aC(i)^b \quad (10)$$

$$\mu(i) = cC(i)^d \quad (11)$$

$$\sigma(i) = \sigma_0 + eC(i)^f \quad (12)$$

where a, b, c, d, e, f are fitting parameters and σ_0 is the surface tension of water.

7. Water potential of the liquid bridge is determined according to Equation 2 at each iteration.
8. For the successive pore drainage, we consider three stages:
 - 8.1. For $|r_2| > |r_1|$, when the capillary pressure h_{cap} is negative, the spatial configuration of the liquid phase in the pore space is obtained by successively applying morphological opening operation on the water-filled space with decreasing diameter of the spherical structuring element followed by steps 4–7 (e.g., Figure 5).
 - 8.2. When $|r_2| < |r_1|$ (i.e., h_{cap} becomes positive) and $Oh < 1$, the capillary bridge is rapidly drained and breaks up.
 - 8.3. When $|r_2| < |r_1|$ and $Oh > 1$, the liquid bridge thins at a rate calculated according to Equation 4. During thinning, the absorption potential h_{ab} becomes increasingly negative and h_{cap} can become positive. The spontaneous thinning of the liquid bridge continues until the water potential, calculated based on Equation 2, is equal or more negative than the water potential derived in the previous steps.

9. For the liquid configuration derived in steps 3 and 8 friction between concentrated mucilage at the gas-liquid interface and particle surfaces is calculated to check whether the interface could move to the newly calculated configuration. To do so, we calculate the local velocity at the gas-liquid interface $v(R)$ for each iteration based on the change in liquid volume assuming a constant drying rate Q defined as the change in soil water content $[d\theta]$ per time $[dt]$. Equation 8 is solved analytically to test if the liquid-gas interface can retreat or if friction would prevent its movement resulting in the creation of a solid 2D penular structure. If Equation 8 allows a solution, then the network can recede with the bulk of the liquid. Else, if Equation 8 does not allow a (real) solution, the polymers are deposited at the gas-liquid interface.

4. Experimental Methods

4.1. Mucilage Collection

Maize seeds (*Zea mays* L., KWS 2376) were sterilized with 10% H_2O_2 solution for 10 min and germinated on PVC meshes under high humidity conditions above aerated water in closed boxes. A detailed description is found elsewhere (Holz et al., 2018). Hydrated mucilage was collected from emerging roots after 3 days of growth at about 20°C. Gel was sucked from root tips through a silicon tube into a glass vial by applying negative pressure. The initial concentration was derived by oven drying 3 g of hydrated gel. Initial concentration of mucilage after the collection was 1.6 mg g⁻¹ (standard deviation: 0.35 mg g⁻¹).

Chia seed mucilage was extracted similar to the description of Benard, Zarebanadkouki, Hedwig, et al. (2018) by mixing seeds at a gravimetric ratio of 1:10 with deionized water. After two hours, mucilage and seeds were separated by passing the mixture through 0.5 and 0.2 mm sieves by applying -800 hPa.

4.2. Quantification of Mucilage Water Potential

Water potential of hydrated mucilage at different concentrations was measured using a dew point technique (WP4C Dewpoint PotentiaMeter, METER Group, Inc. USA). Three samples of mucilage of 5.8–6.6 g and initial concentrations between 2.6 and 2.8 mg g⁻¹ were measured repeatedly after intervals of air drying to cover a range of concentrations from 4 to 180 mg g⁻¹ and potentials between ~0 MPa and >-2 MPa. The procedure was repeated accordingly for five samples of chia seed mucilage (6–8 g initial weight) with initial concentrations ranging from 5.8 to 7.5 mg g⁻¹ to cover a range of water potentials of ~0 MPa to >-0.6 MPa for concentrations between 5.8 and 40 mg g⁻¹.

4.3. Quantification of Mucilage Viscosity and Surface Tension

Measurements of viscosity were conducted with an extensional rheometer (HAAKE CaBER 1, Thermo Scientific, Germany) with the program Thermo Haake CaBER V5.0.12.0 Analysis and Thermo Haake CaBER V5.0.12.0 Control (Cambridge Polymer Group 2001–2015). Mucilage was diluted with deionized water or concentrated by air drying to derive concentrations of 2, 4 and 10 mg g⁻¹ for maize mucilage and 2, 4, 8, and 10 mg g⁻¹ for chia seed mucilage. 35 μ L of hydrated gel was loaded into the initial gap (1.5 mm) between two steel plates with diameter 6 mm using a pipette. Strike distance and time were 6.99 mm and 300 ms, respectively. Surfaces were cleaned with acetone before and after each measurement. Viscosity was estimated taking the linear part of the relation between filament radius and time according to the procedure described by Sattler et al. (2012). Although mucilage is shear thinning (Naveed et al., 2019), a constant viscosity gave a satisfying match of the thinning curve.

Surface tension must be known to determine viscosity and it was measured for chia mucilage up to a concentration of 5 mg g⁻¹ and for maize mucilage up to a concentration of 10 mg g⁻¹ employing the pendant drop method (Drop Shape Analyzer, DSA25S, with ADVANCE software, Krüss GmbH, Germany).

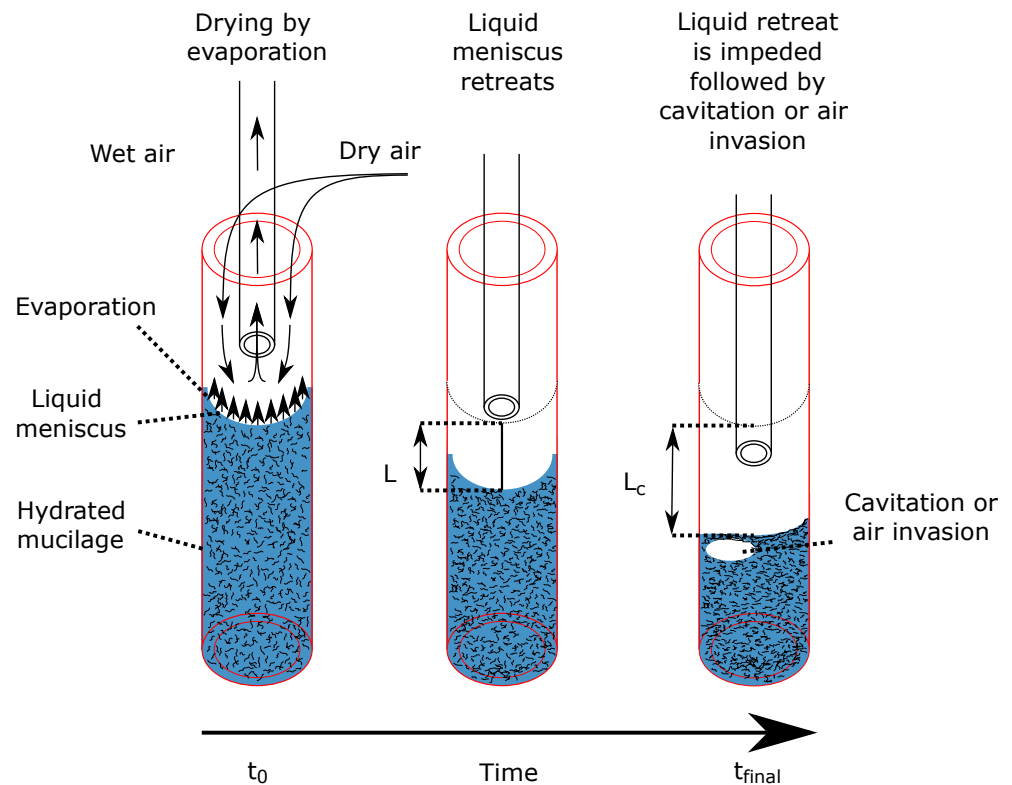


Figure 6. Experimental setup of evaporation-driven liquid retreat in glass capillaries. The speed of evaporation-driven retreat of a liquid meniscus is induced by a constant flow of dry air above the gas-liquid interface. Air is removed through a blunt syringe moving toward the meniscus at a constant velocity equal to the velocity of liquid retreat.

4.4. Quantification of Mucilage Structure Extent in Porous Media

Hydrated chia and maize mucilage at concentrations of 5.6 and 13.9 mg g⁻¹ were mixed with glass beads (SWARCO VESTGLAS GmbH, Germany) of 0.1–0.2 mm in diameter and spread as a thin layer (1.5 ± 0.1 mm) on glass slides (Menzel Gläser, Thermo scientific, Germany). The porous medium was let dry by evaporation within 3 h.

Dry mucilage structures were stained by immersion in a 1:10 deionized water-ink solution (Tinte 4001, Pelikan, Germany) for 10 s and subsequent immersion in deionized water to remove excess ink. After air drying for 24 h at ambient humidity, width and length of stained mucilage structures were measured using a microscope equipped with a digital camera and dedicated software (Axio Imager 2, AxioCam 305, Zen 2 core, Carl Zeiss, Germany). Width and length of mucilage structures were analyzed at 5 random positions with size of 1,346 μm * 1,612 μm on 3 slides. The width of structures was measured at mid distance between particles and the length of a structure was measured perpendicular to its width.

4.5. Verification of the Impact of Drying Rate on Mucilage Structure Formation

To test a central hypothesis of the model, according to which friction and the velocity of the gas-liquid interface trigger the formation of two-dimensional surfaces, we performed experiments in glass capillaries. Experiments in capillaries allow one to control the velocity of the meniscus more easily, while even in simplified geometries such as glass beads this remains challenging. The capillaries had an inner diameter of 0.8 mm and were filled with chia seed mucilage of 6.5 mg g⁻¹ in initial concentration using a syringe. Their lower end was sealed with laboratory fat to avoid air invasion. By sucking humid air from above the liquid meniscus using a blunt syringe of 0.2 mm in diameter and providing dry air to this region via a tube connected to a reservoir of silica gel (Silica gel orange; ROTH AG), the retreat of the liquid meniscus was induced. By lowering the syringe at a constant rate, a constant retreat of the liquid as depicted in Figure 6

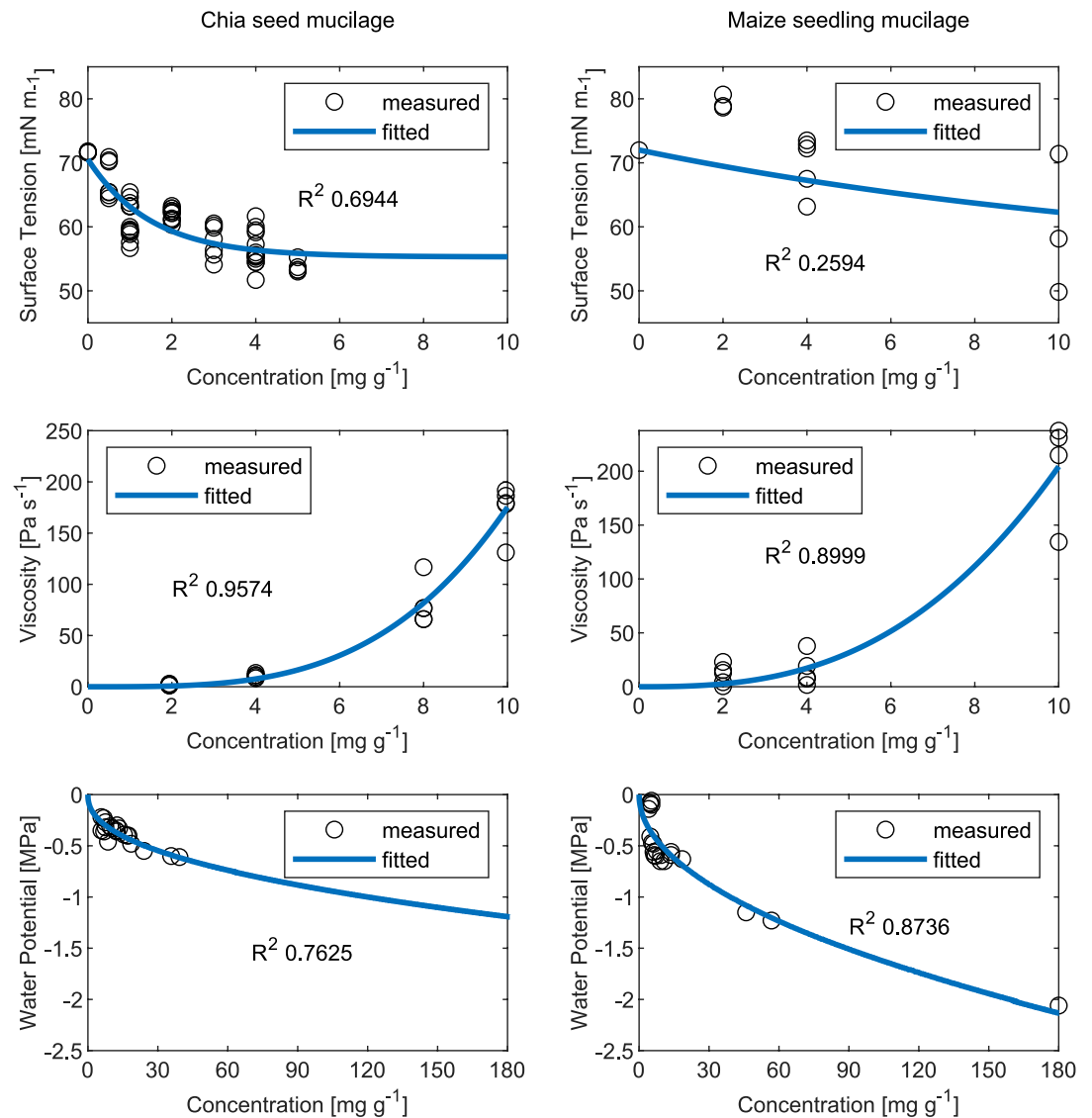


Figure 7. Surface tension, viscosity, and water potential of chia seed (*Salvia hispanica*) mucilage (left) and maize (*Zea mays* L.) mucilage (right) vs. concentration. Measured (black circles) and fitted (blue lines) properties. From top to bottom: surface tension, viscosity and water potential.

was initiated. The process was recorded using the Drop Shape Analyzer Camera and Software (DSA25S, with ADVANCE software, Krüss GmbH, Germany). The time series was analyzed using MATLAB (Version 2018b [MATLAB, 2018]; The MathWorks inc.) by segmenting liquid and air and fitting a circle matching the interface curvature at each time step. The critical length, L_c when the liquid retreat was stopped was derived for the time when the radius of the fitted circle decreased from its initial radius of ca. 0.6 mm to a value below 0.22 mm. At this point, the liquid retreat was altered by a polymeric layer formed at the gas-liquid interface and air entered through this structure by invasion across the network or by cavitation. A representative visualization of the process and the fitting procedure can be found in Movie S1.

5. Results

Viscosity, water potential and surface tension of mucilage collected from chia seeds and maize seedling roots followed the expected behavior. With an increase in mucilage concentration, viscosity increased, and water potential and surface tension decreased (Figure 7). Power law parameterizations were used to fit

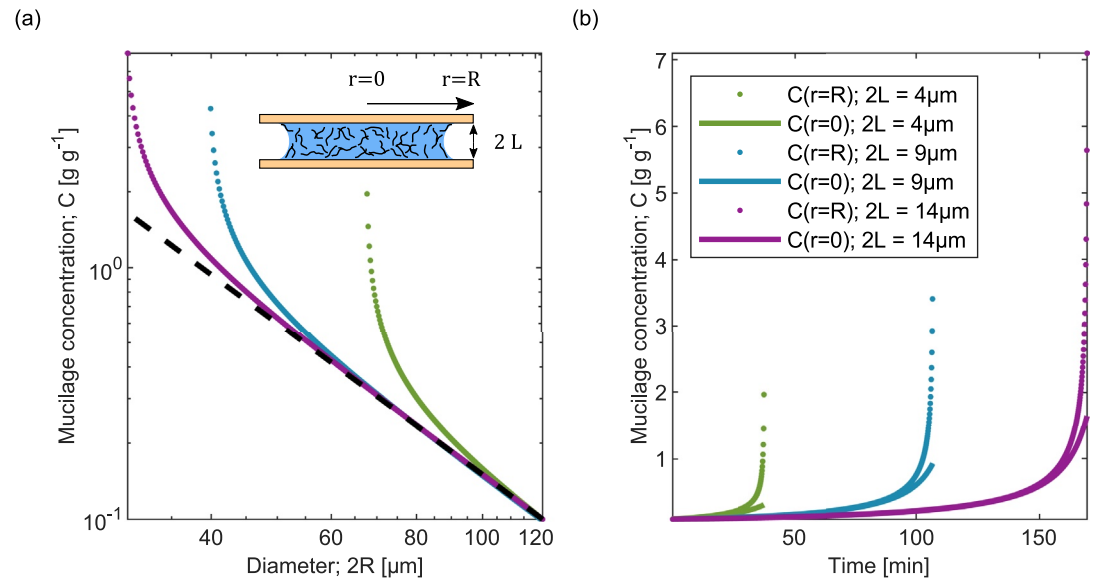


Figure 8. Mucilage concentration at the center ($C(r = 0)$) and at the liquid-gas interface ($C(r = R)$); (a) C (mucilage concentration) over $2R$ (diameter of the liquid bridge) and (b) C (mucilage concentration) over time for $2L$ of 4 μm (green), 9 μm (blue) and 14 μm (purple) at $r = 0$ (solid lines) and $r = R$ (dotted lines). Initially $C(r = R)$ is close to $C(r = 0)$, then during drying the two values diverge. There is a critical point when $C(r = R)$ increases asymptotically. At this point the polymers are deposited forming hollow cylinders. The curves are obtained by solving analytically Equation 8.

the curves for viscosity and water potential (Equations 9 and 10). With increase in concentration from 0 to 10 mg g⁻¹, viscosity increased by two orders of magnitude to about 200 Pa s⁻¹ for both, chia seed and maize seedling mucilage. The derived fit of water potential as function of mucilage concentration indicates a stronger decrease in water potential for maize seedling mucilage compared to chia seed mucilage. Measures of surface tension of both mucilages showed a similar behavior with a decrease in surface tension with increasing concentration as reported in the literature (Naveed et al., 2019; Read & Gregory, 1997).

Variations within quantities of all parameters are partly explained by the heterogeneous composition of mucilage within a single sample. For low concentrations, the impact of such variations is small while after samples were dried to yield higher concentrations, observed differences are amplified.

The exemplary analytical simulation results presented in Figure 8 illustrate the impact of particle distance, $2L$, on the evolution of mucilage concentration at the center ($r = 0$) and at the gas-liquid interface ($r = R$) of a pendular liquid bridge between two plates as calculated using Equation 8. Complete drying within 3 h and an initial mucilage concentration of 0.1 g g⁻¹ were assumed. For the physical properties derived for maize seedling mucilage (i.e., Figure 7), the model predicts an asymptotic increase in concentration at larger liquid bridge diameter ($2R$, Figure 8a) and at an earlier time (Figure 8b) for a decrease in particle distance (green line).

Numerical simulation results for maize seedling and chia seed mucilage between sphere pairs are presented in Figure 9. The size of mucilage structures formed in drying glass beads at initial concentrations of 5.6 and 13.9 mg g⁻¹ are plotted along simulation results. Final diameter and length of structures increased with increasing initial concentration, in both the measurements and simulations. Extent of measured structures appeared scattered, yet with a clear trend for longer and wider bridges at higher initial concentration. While chia seed mucilage formed filaments at low and high initial concentration, this tendency was not observed for maize mucilage. For experimentally derived physical properties, the model well predicted filaments at both initial mucilage concentrations and for both types of mucilage. The trend for larger structures at small particle distances was captured by the model.

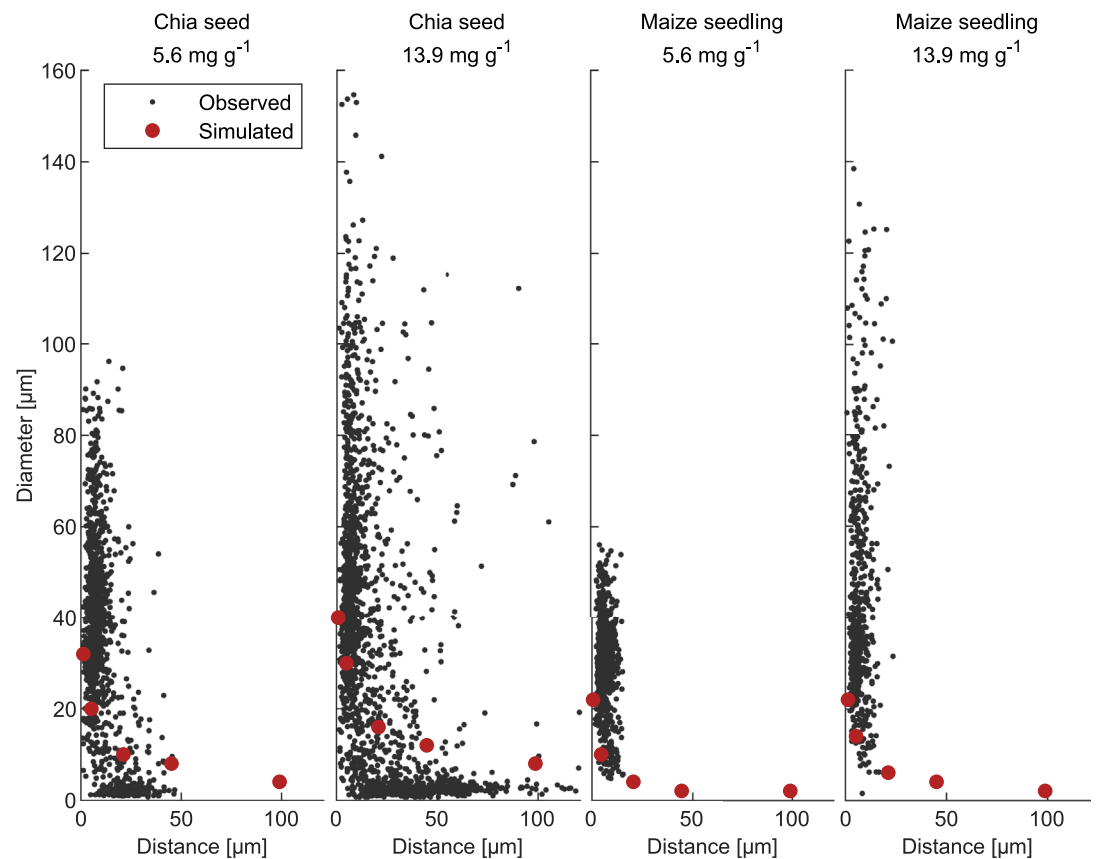


Figure 9. Measured (gray dots) and simulated (red dots) diameter of dry mucilage structures between glass beads (0.1–0.2 mm in diameter) for initial mucilage concentrations of 5.6 and 13.9 mg g⁻¹.

Measurements of critical length (L_c) of liquid retreat using glass capillaries showed a tendency for earlier structure formation (i.e., impedance of liquid retreat) at high velocities with one exception of comparably early deposition at low velocity (0.9 mm at 1.6 $\mu\text{m s}^{-1}$; Figure 10).

Local polymer concentration and velocities of retreating menisci in porous media are non-uniform due to the irregular nature of the drainage process. Employing the simplified geometry of capillaries allowed to bypass these irregularities and to quantify the impact of velocity hence friction on the retreat of hydrated mucilage. The results support our assumption to treat the polymeric blend as a viscous material confirming the contribution of friction in the creation of continuous polymeric structures.

6. Discussion

The interplay of capillary, viscous, and absorptive forces explains the different types of liquid bridges created by polymeric blends in soil. At high mucilage concentration, absorptive forces dominate over capillary forces preserving the integrity of liquid pendular bridges during drying. At low mucilage concentration, surface tension lowers capillary forces and facilitates air entry. For water, surface tension causes rapid drainage and breakup of the liquid connection. For polymer solutions, viscosity controls the thinning rate of a pendular bridge and eventually prevents its breakup.

High viscosity of polymer solutions also explains the formation of 2D structures such as hollow cylinders between two solid particles. To predict the size of 2D structures, we included the impact of friction in a model of drying polymer solutions in porous media. The model compares the key forces acting on the polymer network, which are water absorption of the polymer network and the resistance to flow. The first force drives the network toward the center of a liquid bridge (from high to low concentrations), the second force describes the resistance to this flow. Equating the two forces, we calculated the critical point when

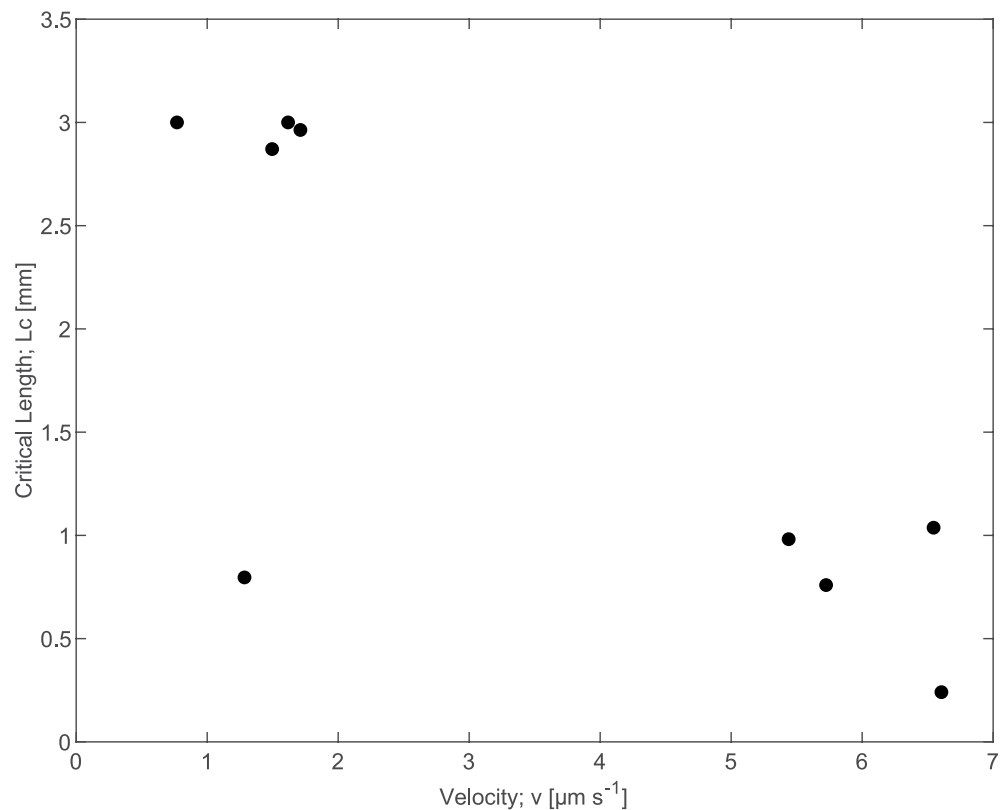


Figure 10. Critical drying length, L_c as function of velocity of the gas-liquid interface in evaporation experiments. Capillaries were filled with chia seed mucilage at an initial concentration of 5.6 mg g^{-1} .

friction impedes the receding of the polymer network. Simulation results proof the capability of the model to predict the formation of thin filaments and 2D hollow cylinders. Despite its simplicity, the model can predict the tendency for larger 2D structures at high initial concentration observed from drying experiments in glass beads. The trend for wider structures forming between closer particles and narrower and longer structured between distant particles (as visible in Figure 1a) was captured. The model shows that viscosity and water absorption are key properties determining the drying dynamics of polymer solutions in porous media. The impact of specific surface of the porous medium (here expressed by the distance between particles $2L$) contributes to the critical concentration at which the polymers are deposited which was captured by the model.

Predicted diameters of polymeric structures were generally smaller than observed in glass beads. One reason for this deviation originates from the restricted dimensions of the employed model to the inter-particle space and the geometry of pendular liquid bridges. This spatial limitation only allows to predict structures of a diameter smaller than particles. Additionally, high velocities can be expected in a multi-pore environment due to the rapid drainage of large pores. On the other hand, for pendular bridges, rapid drainage occurs just before breakup of the liquid phase resulting in the creation of thin thread-like structures at high viscosities as captured by the model. Results of drying experiments using capillaries support the rate dependency of the process. At high velocities, an earlier deposition of polymeric structures was observed hence larger structures can be expected at high velocities of the gas-liquid interface in multi-porous environments like soil as well.

Presented results apply to root mucilage and EPS produced by soil microorganisms, which form 1D and 2D structures in soils as previously reported (Albalasmeh & Ghezzehei, 2014; Benard et al., 2019; Zheng et al., 2018).

The implications of these structures are diverse. After its deposition, the polymer network can further enhance water retention by acting as a new solid matrix preventing or delaying the air entry. This new matrix

maintains the connectivity of the liquid phase, thus enhancing the unsaturated hydraulic conductivity (Benard et al., 2019) and the diffusion coefficient in soils (Zarebanadkouki et al., 2019), and it reduces gas diffusion (Haupenthal et al., 2021), thus reducing evaporative fluxes. Additionally, the formation of extensive 2D structures corresponds to a sudden increase in soil water repellency, which reduces the rewetting kinetics (Benard, Zarebanadkouki, & Carminati, 2018). In summary, these structures can buffer fluctuations in soil water content and fluxes, protecting soil organisms against the consequences of fluctuating soil water content, thus, enabling extended periods of biological activity or hot moments (Kuzuyakov & Blagodatskaya, 2015) in soil.

It is without question that the presented experimental data and evidence were made in simplified porous environments. This was required to test the concept, as the identification and quantification of polymeric structures in undisturbed soil still poses a major challenge. So far, only few examples of the discussed polymeric structures from natural systems, like biocrust (e.g., Figures 2a and S5 from Benard et al., 2019) or semi-natural systems, like bacteria grown in sand (e.g., Figure 6 from Zheng et al., 2018) have been reported. The lack of evidence is related to the elusive nature of the polymeric blends of EPS and mucilage, which can hardly be distinguished from soil water and occupy comparably little space after desiccation. Nevertheless, our concept is capable to predict the effect of polymeric substances released by soil organisms on the physical properties of soil water and its interactions with porous media, regardless of the complexity of the pore space.

The key ingredient for mucilage and EPS to shape the liquid phase is their high viscosity and water absorption. Counterintuitively, the high viscosity is expected to result in a greater hydraulic conductivity and diffusivity (in the liquid phase) in drying soils.

Data Availability Statement

The data presented in Figures 7, 9 and 10 are available from <https://doi.org/10.6084/m9.figshare.14292305.v2>.

Acknowledgments

This project was carried out in the framework of the priority program 2089 “Rhizosphere spatiotemporal organization—a key to rhizosphere functions” funded by the German Research Foundation DFG under the project number 403640522. Imaging of maize mucilage distribution in glass beads was conducted at SLS (Swiss Light Source) facility of the PSI, Switzerland. Open access funding provided by Eidgenössische Technische Hochschule Zurich.

References

- Albalasmeh, A. A., & Ghezzehei, T. A. (2014). Interplay between soil drying and root exudation in rhizosheath development. *Plant and Soil*, 374(1–2), 739–751. <https://doi.org/10.1007/s11104-013-1910-y>
- Arand, F., & Hesser, J. (2017). Accurate and efficient maximal ball algorithm for pore network extraction. *Computers & Geosciences*, 101, 28–37. <https://doi.org/10.1016/j.cageo.2017.01.004>
- Benard, P., Zarebanadkouki, M., Brax, M., Kaltenbach, R., Jerjen, I., Marone, F., et al. (2019). Microhydrological niches in soils: How mucilage and EPS alter the biophysical properties of the rhizosphere and other biological hotspots. *Vadose Zone Journal*, 18(1), 1–10. <https://doi.org/10.2136/vzj2018.12.0211>
- Benard, P., Zarebanadkouki, M., & Carminati, A. (2018). Impact of pore-scale wettability on rhizosphere rewetting. *Frontiers in Environmental Science*, 6, 16. <https://doi.org/10.3389/fenvs.2018.00016>
- Benard, P., Zarebanadkouki, M., Hedwig, C., Holz, M., Ahmed, M. A., & Carminati, A. (2018). Pore-scale distribution of mucilage affecting water repellency in the rhizosphere. *Vadose Zone Journal*, 17(1), 1–9. <https://doi.org/10.2136/vzj2017.01.0013>
- Bengough, A. G. (2012). Water dynamics of the root zone: Rhizosphere biophysics and its control on soil hydrology. *Vadose Zone Journal*, 11(2), vzj2011.0111. <https://doi.org/10.2136/vzj2011.0111>
- Carminati, A., Benard, P., Ahmed, M. A., & Zarebanadkouki, M. (2017). Liquid bridges at the root-soil interface. *Plant and Soil*, 417, 1–15. <https://doi.org/10.1007/s11104-017-3227-8>
- Chan, T. P., & Govindaraju, R. S. (2011). Pore-morphology-based simulations of drainage and wetting processes in porous media. *Hydrology Research*, 42(2–3), 128–149. <https://doi.org/10.2166/nh.2011.058>
- Eggers, J., & Villermaux, E. (2008). Physics of liquid jets. *Reports on Progress in Physics*, 71(3), 036601. <https://doi.org/10.1088/0034-4885/71/3/036601>
- Flemming, H.-C., & Wingender, J. (2001). Relevance of microbial extracellular polymeric substances (EPSs)—Part I: Structural and ecological aspects. *Water Science and Technology*, 43(6), 1–8. <https://doi.org/10.2166/wst.2001.0326>
- Flemming, H.-C., & Wingender, J. (2010). The biofilm matrix. *Nature Reviews Microbiology*, 8(9), 623–633. <https://doi.org/10.1038/nrmicro2415>
- Flemming, H.-C., Wingender, J., Szewzyk, U., Steinberg, P., Rice, S. A., & Kjelleberg, S. (2016). Biofilms: An emergent form of bacterial life. *Nature Reviews Microbiology*, 14(9), 563–575. <https://doi.org/10.1038/nrmicro.2016.94>
- Haupenthal, A., Brax, M., Bentz, J., Jungkunst, H. F., Schützenmeister, K., & Kroener, E. (2021). Plants control soil gas exchanges possibly via mucilage. *Journal of Plant Nutrition and Soil Science*, 184(3), 320–328. <https://doi.org/10.1002/jpln.202000496>
- Hilpert, M., & Miller, C. T. (2001). Pore-morphology-based simulation of drainage in totally wetting porous media. *Advances in Water Resources*, 24(3–4), 243–255. [https://doi.org/10.1016/S0309-1708\(00\)00056-7](https://doi.org/10.1016/S0309-1708(00)00056-7)
- Holz, M., Leue, M., Ahmed, M. A., Benard, P., Gerke, H. H., & Carminati, A. (2018). Spatial distribution of mucilage in the rhizosphere measured with infrared spectroscopy. *Frontiers in Environmental Science*, 6, 87. <https://doi.org/10.3389/fenvs.2018.00087>

- Kuzyakov, Y., & Blagodatskaya, E. (2015). Microbial hotspots and hot moments in soil: Concept & review. *Soil Biology and Biochemistry*, 83, 184–199. <https://doi.org/10.1016/j.soilbio.2015.01.025>
- MATLAB. (2018). *Version 9.5 (R2018b)*. The MathWorks Inc.
- McClain, M. E., Boyer, E. W., Dent, C. L., Gergel, S. E., Grimm, N. B., Groffman, P. M., et al. (2003). Biogeochemical hot spots and hot moments at the interface of terrestrial and aquatic ecosystems. *Ecosystems*, 6(4), 301–312. <https://doi.org/10.1007/s10021-003-0161-9>
- McCully, M. E., & Boyer, J. S. (1997). The expansion of maize root-cap mucilage during hydration. 3. Changes in water potential and water content. *Physiologia Plantarum*, 99(1), 169–177. <https://doi.org/10.1111/j.1399-3054.1997.tb03445.x>
- McKinley, G. H., & Tripathi, A. (2000). How to extract the Newtonian viscosity from capillary breakup measurements in a filament rheometer. *Journal of Rheology*, 44(3), 653–670. <https://doi.org/10.1122/1.551105>
- Naveed, M., Ahmed, M. A., Benard, P., Brown, L. K., George, T. S., Bengough, A. G., et al. (2019). Surface tension, rheology, and hydrophobicity of rhizodeposits and seed mucilage influence soil water retention and hysteresis. *Plant and Soil*, 437(1–2), 65–81. <https://doi.org/10.1007/s11104-019-03939-9>
- Naveed, M., Brown, L. K., Raffan, A. C., George, T. S., Bengough, A. G., Roose, T., et al. (2017). Plant exudates may stabilize or weaken soil depending on species, origin and time: Effect of plant exudates on rhizosphere formation. *European Journal of Soil Science*, 68(6), 806–816. <https://doi.org/10.1111/ejss.12487>
- Ohnesorge, W. V. (1936). Die bildung von tropfen an düsen und die auflösung flüssiger strahlen. *ZAMM-Journal of Applied Mathematics and Mechanics/Zeitschrift Für Angewandte Mathematik Und Mechanik*, 16(6), 355–358. <https://doi.org/10.1002/zamm.19360160611>
- Raaijmakers, J. M., De Bruijn, I., Nybroe, O., & Ongena, M. (2010). Natural functions of lipopeptides from *Bacillus* and *Pseudomonas*: More than surfactants and antibiotics. *FEMS Microbiology Reviews*, 34(6), 1037–1062. <https://doi.org/10.1111/j.1574-6976.2010.00221.x>
- Read, D. B., Bengough, A. G., Gregory, P. J., Crawford, J. W., Robinson, D., Scrimgeour, C. M., et al. (2003). Plant roots release phospholipid surfactants that modify the physical and chemical properties of soil. *New Phytologist*, 157(2), 315–326. <https://doi.org/10.1046/j.1469-8137.2003.00665.x>
- Read, D. B., & Gregory, P. J. (1997). Surface tension and viscosity of axenic maize and lupin root mucilages. *New Phytologist*, 137(4), 623–628. <https://doi.org/10.1046/j.1469-8137.1997.00859.x>
- Read, D. B., Gregory, P. J., & Bell, A. E. (1999). Physical properties of axenic maize root mucilage. *Plant and Soil*, 211(1), 87–91.
- Roberson, E. B., Chenu, C., & Firestone, M. K. (1993). Microstructural changes in bacterial exopolysaccharides during desiccation. *Soil Biology and Biochemistry*, 25(9), 1299–1301. [https://doi.org/10.1016/0038-0717\(93\)90230-9](https://doi.org/10.1016/0038-0717(93)90230-9)
- Roberson, E. B., & Firestone, M. K. (1992). Relationship between desiccation and exopolysaccharide production in a soil *Pseudomonas* sp. *Applied and Environmental Microbiology*, 58(4), 1284–1291. <https://doi.org/10.1128/AEM.58.4.1284-1291.1992>
- Sattler, R., Gier, S., Eggers, J., & Wagner, C. (2012). The final stages of capillary break-up of polymer solutions. *Physics of Fluids*, 24(2), 023101. <https://doi.org/10.1063/1.3684750>
- Segura-Campos, M. R., Ciau-Solís, N., Rosado-Rubio, G., Chel-Guerrero, L., & Betancur-Ancona, D. (2014). Chemical and functional properties of chia seed (*Salvia hispanica* L.) Gum. *International Journal of Food Science*, 2014, 1–5. <https://doi.org/10.1155/2014/241053>
- Stoodley, P., Cargo, R., Rupp, C. J., Wilson, S., & Klapper, I. (2002). Biofilm material properties as related to shear-induced deformation and detachment phenomena. *Journal of Industrial Microbiology and Biotechnology*, 29(6), 361–367. <https://doi.org/10.1038/sj.jim.7000282>
- Tuller, M., Or, D., & Dudley, L. M. (1999). Adsorption and capillary condensation in porous media: Liquid retention and interfacial configurations in angular pores. *Water Resources Research*, 35(7), 1949–1964. <https://doi.org/10.1029/1999WR900098>
- Van Rossum, G., & Drake, F. L. (2009). *Python 3 reference manual*. CreateSpace. <https://doi.org/10.1029/1999wr900098>
- Vogel, H.-J., Tölke, J., Schulz, V. P., Krafczyk, M., & Roth, K. (2005). Comparison of a Lattice-Boltzmann model, a full-morphology model, and a pore network model for determining capillary pressure-saturation relationships. *Vadose Zone Journal*, 4(2), 380–388. <https://doi.org/10.2136/vzj2004.0114>
- Walker, T. S., Bais, H. P., Grotewold, E., & Vivanco, J. M. (2003). Root exudation and rhizosphere biology. *Plant Physiology*, 132(1), 44–51. <https://doi.org/10.1104/pp.102.019661>
- Zarebanadkouki, M., Fink, T., Benard, P., & Banfield, C. C. (2019). Mucilage facilitates nutrient diffusion in the drying rhizosphere. *Vadose Zone Journal*, 18(1), 1–13. <https://doi.org/10.2136/vzj2019.02.0021>
- Zheng, W., Zeng, S., Bais, H., LaManna, J. M., Hussey, D. S., Jacobson, D. L., & Jin, Y. (2018). Plant growth-promoting rhizobacteria (PGPR) reduce evaporation and increase soil water retention. *Water Resources Research*, 54, 3673–3687. <https://doi.org/10.1029/2018WR022656>